Computational aspects of DFT, HOMO-LUMO, PED, molecular docking and basic characterisations of Octadec-9-Enoic Acid (C 18 H 34 O 2)

5 authors, including:

C. Prabhu
Vels University
4 PUBLICATIONS   **2** CITATIONS

SEE PROFILE

Rajesh Pv
School of Basic Sciences, Vels Institute of Science Technology & Advanced Studies…
46 PUBLICATIONS   **163** CITATIONS

SEE PROFILE

S. Sahaya Jude Dhas
Kings Engineering College, Chennai
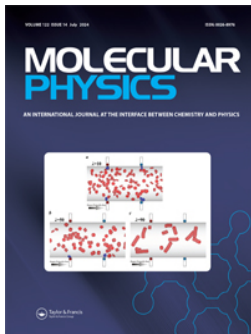**167** PUBLICATIONS   **1,327** CITATIONS

SEE PROFILE

Abdulrahman I Almansour
King Saud University
444 PUBLICATIONS   **3,400** CITATIONS

SEE PROFILE

Computational aspects of DFT, HOMO-LUMO, PED, molecular docking and basic characterisations of Octadec-9-Enoic Acid (C$_{18}$H$_{34}$O$_2$)

C. Prabhu, P. Rajesh, M. Lawrence, S. Sahaya Jude Dhas & Abdulrahman I. Almansour

View supplementary material

Published online: 30 Jul 2024.

Submit your article to this journal

View related articles

View Crossmark data

Taylor & Francis
Taylor & Francis Group

RESEARCH ARTICLE

Check for updates

Computational aspects of DFT, HOMO-LUMO, PED, molecular docking and basic characterisations of Octadec-9-Enoic Acid (C$_{18}$H$_{34}$O$_{2}$)

C. Prabhu[a], P. Rajesh[a], M. Lawrence[a,b], S. Sahaya Jude Dhas[c] and Abdulrahman I. Almansour[d]

[a]Department of Physics, Vels Institute of Science Technology and Advance Studies (VISTAS), Chennai, India; [b]Department of Physics, Loyola Institute of Technology, Chennai, India; [c]Saveetha School of Engineering, Saveetha Institute of Medical and Technical Sciences, Saveetha University, Chennai, India; [d]Department of Chemistry, College of Science, King Saud University, Riyadh, Saudi Arabia

ABSTRACT

Finding a few potential 'green' inhibitors has been a long-term goal because these products that are derived from plants enable prescription drug costs reduced, side effects minimised and biodegradable. Known by its common name, Hybanthusenneaspermus (L.) F. Muell, which is a member of the Violaceae family, is a herb or shrub found worldwide in tropical and subtropical climates. Knowing the applicability of H. enneaspermus for the treatment of a variety of acute or chronic diseases with a diverse nature of phytoconstituents will be made easier with the information provided in this comprehensive article. The majority of the information in this research article was gathered from different scientific sources that focused on H. enneaspermus research. Plant extraction, optimised geometry, thorough vibrational assignment, and characterisation of the fundamental vibrational modes of Octadec-9-Enoic Acid were conducted using experimental FT-IR and UV-Vis data in addition to quantum chemistry research. The actual vibrational data were compared to the wavenumbers computed theoretically for the chemical's optimal shape using DFT/B3LYP gradient calculations with the 6-311G ++ (d,p) basis set. A computation has been performed utilising the energy gap between HOMO and LUMO. Intramolecular interactions (NBO), molecular electrostatic potential (MEP) at a specific point p (x,y,z), atomic charge values, NMR & UV-vis computation, and molecular docking studies with protein-ligand interactions were all interpreted using natural bond orbital analysis.

CONTACT P. Rajesh ✉ rajesh.ncc5coy@gmail.com ▢ Department of Physics, Vels Institute of Science Technology and Advance Studies (VISTAS), Chennai, Tamil Nadu 600117, India; Sahaya Jude Dhas ✉ judedhas@gmail.com ▢ Saveetha School of Engineering, Saveetha Institute of Medical and Technical Sciences, Saveetha University, Chennai, Tamil Nadu, 602105, India
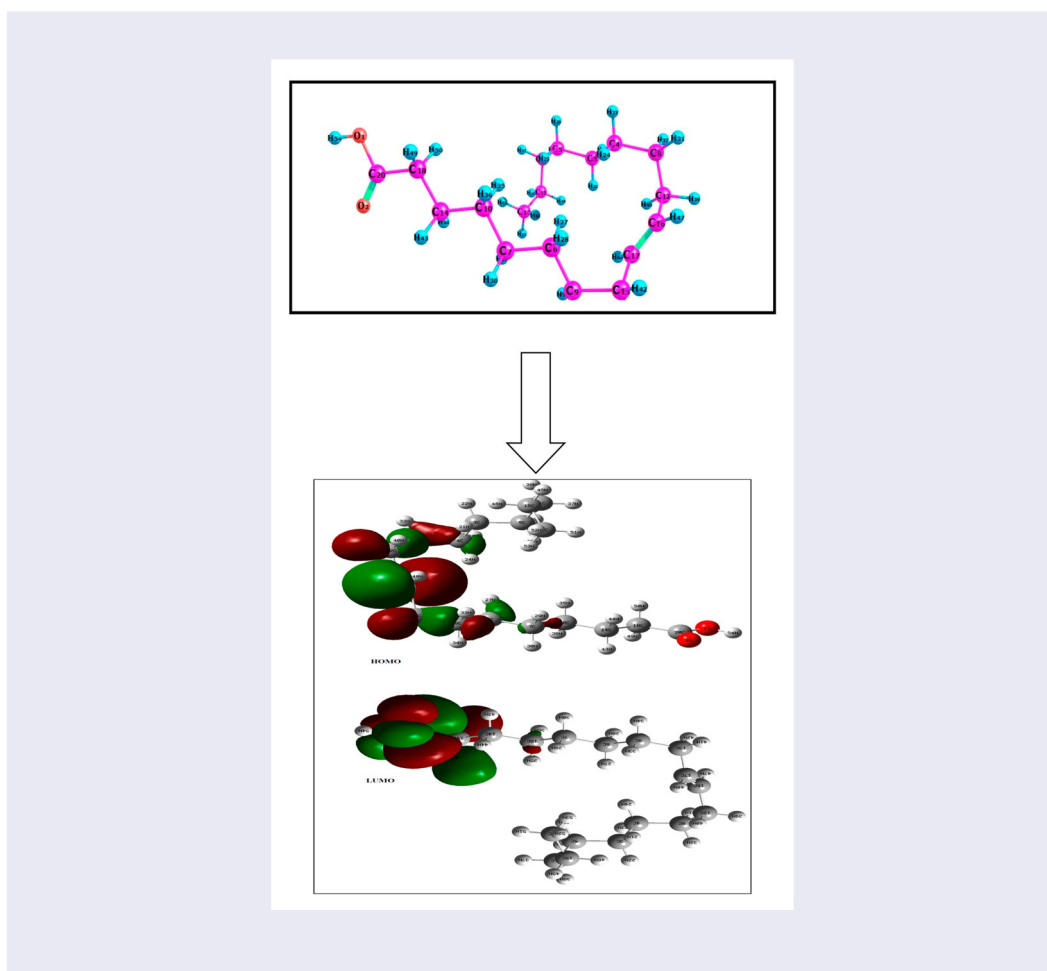
1. Introduction

Over the years, there has been a relentless search to identify an assortment of widely accessible medicinal plants such that the outcomes are on the rise, as using plant-based products reduces the cost and side effects of prescription medications. Finding a few affordable, biodegradable, and powerful 'green' inhibitors is therefore anticipated. On this ground, O9EA, a compound with the molecular formula $C_{18}H_{34}O_2$ and a molecular weight of 282.5 g/mol, is an abundant unsaturated fatty acid that is used as a pharmaceutical solvent. According to some authors' reviews of the literature, phototherapy has been shown to be effective in treating a number of diseases, including inflammation, urinary infections, and compounds that include flavonoids, sugars, tannins, alkaloids, and some psychopharmacological implications [1]. The WHO has identified medicinal plants as a critical component of global health, and they play an indispensable part in healthcare such that they have a variety of beneficial qualities. Rural people use a variety of medicinal plants that are widely available, particularly in developing and underdeveloped countries.

Thousands of medicinal plants have been used in India for medical purposes since ancient times [2]. Synthetic analgesics that are sold commercially have a number of negative effects, including gastrointestinal irritation, constipation, and kidney damage. Utilising products made from plants minimises the expense and negative effects of prescription drugs [3]. Strong growth inhibitory activity against the HEp-2 cell line was demonstrated by anticancer activity [4]. Investigation of the inhibitory action of apricot pomace extract as a green vapour phase corrosion inhibitor of mild steel has contributed significantly [5]. Because of the 'green chemistry' theory that is currently prominent in science, technology, and engineering, the use of conventional corrosion inhibitors is now restricted. This has led researchers to discover a few inexpensive, biodegradable, and potent 'green' inhibitors [6]. The World Health Organisation (WHO) acknowledges medicinal plants as essential to global health and their significant role in healthcare. Hybanthusenneaspermus (L) F. Muell, a vital medicinal herb that has been used for millennia, belongs to the family Violaceae [7]. The plant has been reported for the treatment of 'Kapha' and 'Pitta'
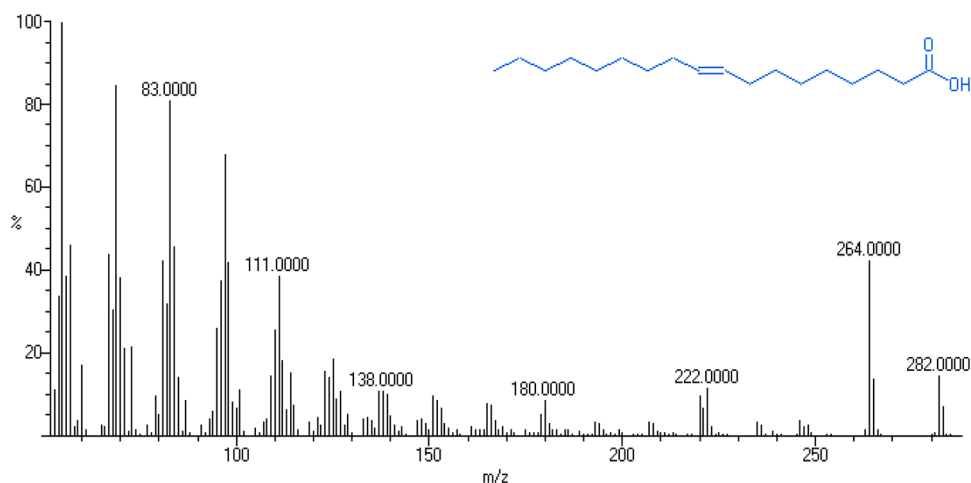
Figure 1. GC-MS Chromatogram of Hybanthusenneaspermus (O9EA)

conditions, urinary calculi, strangury, painful dysentery, vomiting, burning sensation, mental wandering, urethral discharge, blood problems, asthma, epilepsy, coughing, and breast toning in the Ayurvedic literature. The plant's phytochemical composition includes a significant amount of sugars, flavonoids, steroids, triterpenes, phenols, flavones, catechins, tannins, anthraquinones, dipeptide alkaloids, and isoarborinol. According to reports, the plant has pharmacological properties, including scavenging free radicals, hepatoprotective, nephroprotective, aphrodisiac, antiplasmodial, antimicrobial, anticonvulsant, and aldose reductase inhibitory effects. The minimal inhibitory concentration was ascertained by utilising the disc diffusion assay technique to investigate the primary bacteria responsible for urinary tract infections. The ethanol (95%) extract demonstrated substantial contribution and a wider range of inhibition in contrast to the water, which demonstrated a moderate impact; the petroleum ether and chloroform extracts exhibited weak action at 300 mg/disc. The effectiveness of extracts against particular urinary tract infections was compared with that of traditional antibiotics [8].Calculations were performed using density functional theory (DFT) based on DFT/B3LYP with 6-311G ++(d,p) basis set. Molecular docking has been employed to carry out a thorough theoretical and experimental value of FT-IR, GC-MS, UV-Vis spectroscopic investigations, as well as HOMO (Highest Occupied Molecular Orbital) – LUMO (Least Unoccupied Molecular Orbital) for comprehending the chemical stability and reactivity of many organic compounds and Molecular Electrostatic Potential (MEP) analysis has also been performed.

2. Materials and methods

2.1. Plant collection

The required herb of Hybanthusenneaspermus was harvested in its complete form in September in Gingee, Chengalpattu District, Tamilnadu, India.

2.2. Extractions

After thoroughly washing the leaves of Hybanthusenneaspermus in double-distilled water, the leaves were shed and grounded into a 1.0 kg powder, which was then extracted using methanol at room temperature. Using a Soxhlet extractor, methanol extraction was utilised to completely remove the solvent. GC-MS analysis of the crude and extract of the compound revealed the presence of multiple components, as depicted in Figure 1.

2.3. Experimental details

The UV-Vis absorption spectrum was recorded in a spectrophotometer in the range of 200–400 nm, and the experimental and theoretical data of Fourier Transform Infrared (FT-IR) spectra were obtained in the region 4000–400 cm^{-1}.

3. Computational details

Density functional theory (DFT), the Beeke-3-Lee-Yang-Parr (B3LYP) exchange-correlation functional, and 6-311++G (d,p) were employed to optimise the geometry of O9EA in comprehensive detail [9]. The software package Gaussian 09W was utilised for all theoretical
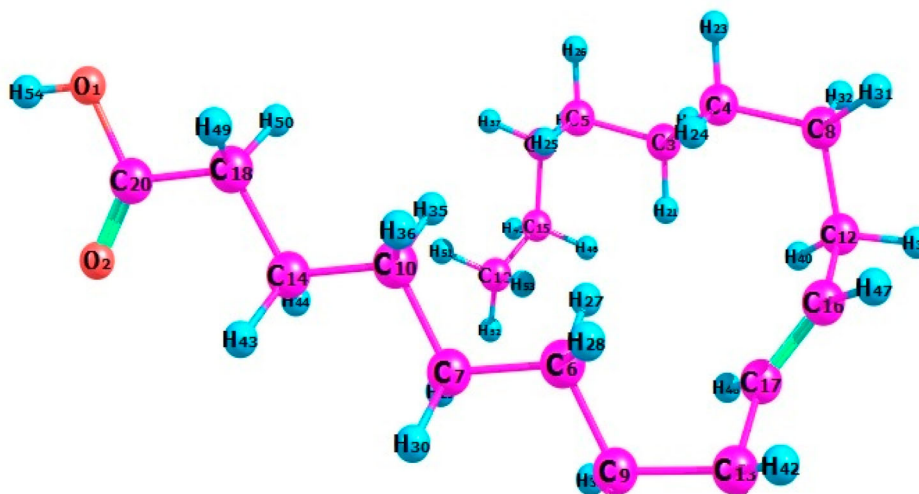
Figure 2. Optimized Structure of O9EA.

calculations [10]. The LANL2DZ basis set [11]-based Chemcraft 1.6 was employed to obtain the molecular structure. The UV-visible spectra, electronic transitions, and other electronic properties like HOMO-LUMO and energy gap were all calculated using the DFT approach. It was also implemented the HOMO and LUMO analyses to learn more about the internal charge transport of the molecule. The potential energy distribution (PED) was computed using the VEDA 4 (Vibrational Energy Distribution Analysis) programme in order to validate the vibrational band allocations [12].

4. Results and discussion

4.1. Optimised geometry

The ChemDraw programme has been utilised to generate the drawing of the molecular structure of NAEF. The precise optimised shape and electronic properties of the NAEF molecule can be found by using the least energy structure optimisation method with DFT and the basis set 6-311++G(d,p) [13]. The O9EA ($C_{18}H_{34}O_2$) has a series of optimised structural values that are listed in the Table S1 of the supplementary section. Figure 2 illustrates the structure and the numbers of Carbon (C), Hydrogen (H), and Oxygen (O) that are present thereby B3LYP 6-311++G (d,p) provides the theoretical value [14].

The optimised structure of bond length in O_1–H_{54} is at about $0.969\,Å$ which has a weak bond whereas C_8–C_{12} possesses a strong bond and has a bond length at about $1.544\,Å$. The theoretical values of bond length for O_1-C_{20}, O_1-H_{54}, O_2-C_{20}, C_{10}-H_{55}, C_{10}-H_{56}, and C_{11}-C_{15} are $1.357, 0.969, 1.204, 1.097, 1.098$, and 1.538, respectively.

Table 1. NBO analysis of O9EA.

Donor NBO (i)	Acceptor NBO (j)	E(2) Kcal / mol	E(j)–E(i) a.u.	F(i,j) a.u.
$\sigma\,C_{13}$–C_{17}	$\sigma^*\,C_{12}$–C_{16}	4.01	1.06	0.058
$\sigma\,C_{12}$–C_{16}	$\sigma^*\,C_{13}$–C_{17}	4.05	1.06	0.059
$\sigma\,C_{13}$–H_{41}	$\pi^*\,C_{16}$–C_{17}	4.16	0.54	0.043
$\sigma\,C_{12}$–H_{39}	$\pi^*\,C_{16}$–C_{17}	4.25	0.54	0.043
$\sigma\,C_{18}$–H_{50}	$\pi^*\,O_2$–C_{20}	4.88	0.51	0.047
$\sigma\,C_{18}$–H_{49}	$\pi^*\,O_2$–C_{20}	5.20	0.51	0.048
$\sigma\,C_{17}$–H_{48}	$\sigma^*\,C_{16}$–H_{47}	5.37	0.94	0.064
LPO_1	$\sigma^*\,O_2$–C_{20}	6.55	1.2	0.079
LPO_2	$\sigma^*\,C_{18}$–C_{20}	17.22	0.65	0.096
LPO_2	$\sigma^*\,O_1$–C_{20}	31.6	0.61	0.125
LPO_1	$\pi^*\,O_2$–C_{20}	44.64	0.34	0.111

4.2. Spectral analysis

Vibrational levels of the compound is analyzed and the investigation's main objective is to determine the non-linear modes (NLM) using the formula (3N-6), where O9EA ($C_{18}H_{34}O_2$) has 156 modes and 54 atoms overall [15,16]. DFT can be used to find the IR bands in spectral analysis using the functional key of B3LYP 6-311++G (d,p). Table 2 contains the percentage value of the potential energy distribution (PED) using the Vibrational Energy Distribution Analysis (VEDA 4) key B3LYP/6-311++G (d,p). Figure 3a and b depict the vibrational Assignment of O9EAin terms of theoretical and experimental based on FT-IR and FT-RAMAN values [17].

4.2.1. Methyl group

The methyl group, or CH_3 in the chemical formula, is a functional group that is derived from methane and consists of one carbon atom bound to three hydrogen atoms. In an aromatic ring, methyl groups are always an

(a)

(b)

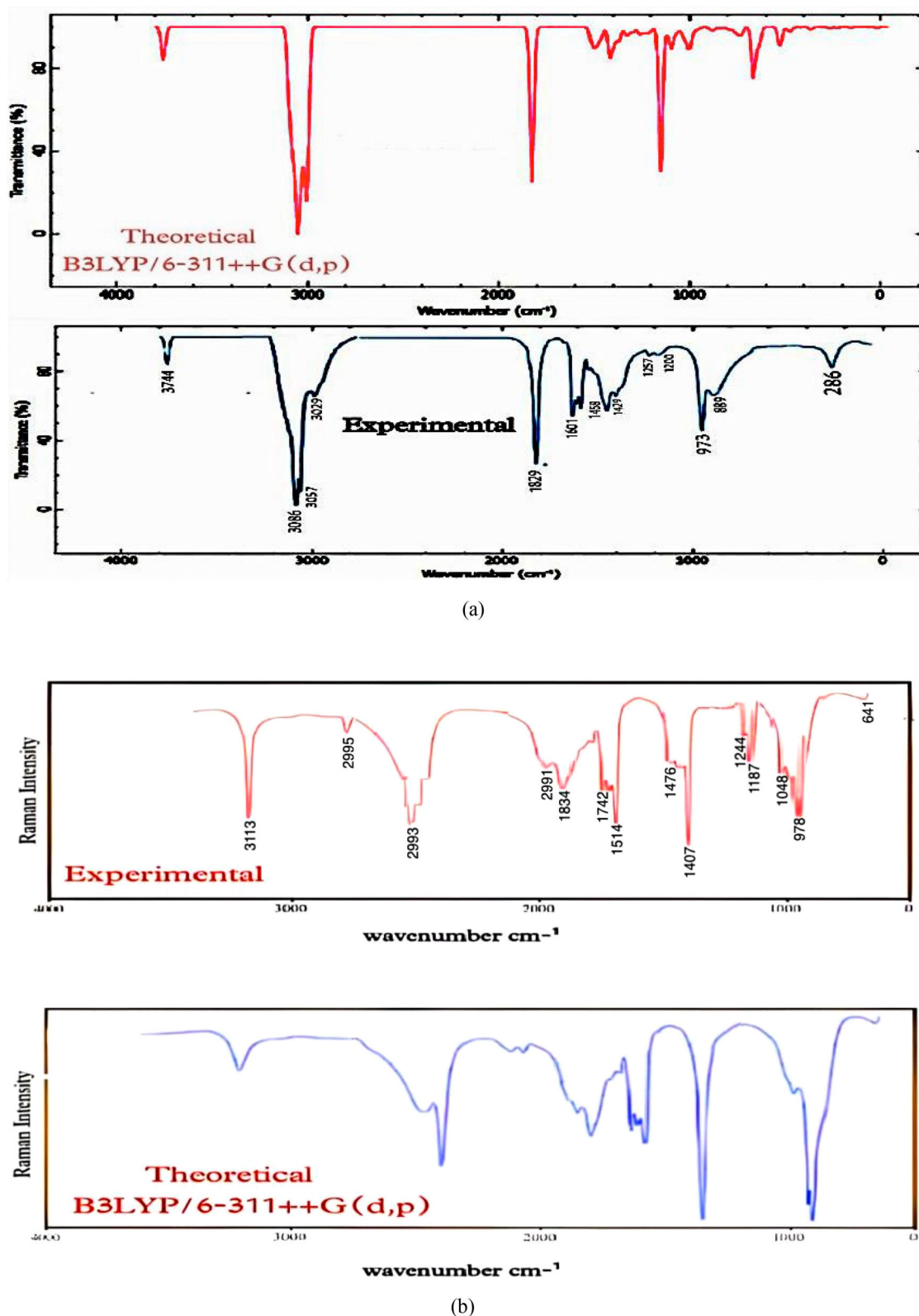**Figure 3.** a. Vibrational Assignment of O9EA (FT-IR). b.Vibrational Assignment of O9EA (FT-RAMAN).

electron-donating substituent [18,19].In any compound, the presence of a methyl group results in the formation of two asymmetric stretching vibrations and one symmetric stretching vibration [20,21]. The wavenumber of the asymmetric stretch is typically higher than that of the symmetric stretch. The asymmetric stretching vibrations

Table 2. Analysis Chargesof O9EA.

Atoms	Charges (eV)	Atoms	Charges(eV)	Atoms	Charges(eV)	Atoms	Charges (eV)
O_1	−0.3314	C_{14}	−0.1971	H_{28}	0.0957	H_{41}	0.1182
O_2	−0.3312	C_{15}	−0.2275	H_{29}	0.1040	H_{42}	0.1021
C_3	−0.2050	C_{16}	−0.1102	H_{30}	0.1028	H_{43}	0.1180
C_4	−0.2055	C_{17}	−0.1113	H_{31}	0.1042	H_{44}	0.1183
C_5	−0.2170	C_{18}	−0.2611	H_{32}	0.1030	H_{45}	0.1075
C_6	−0.2046	C_{19}	−0.2995	H_{33}	0.1017	H_{46}	0.1049
C_7	−0.2032	C_{20}	0.34822	H_{34}	0.1047	H_{47}	0.0823
C_8	−0.2205	H_{21}	0.11049	H_{35}	0.1052	H_{48}	0.0838
C_9	−0.2185	H_{22}	0.09775	H_{36}	0.1009	H_{49}	0.1412
C_{10}	−0.2103	H_{23}	0.10238	H_{37}	0.1029	H_{50}	0.1416
C_{11}	−0.2087	H_{24}	0.11708	H_{38}	0.1043	H_{51}	0.1017
C_{12}	−0.1933	H_{25}	0.10807	H_{39}	0.1187	H_{52}	0.1069
C_{13}	−0.1924	H_{26}	0.10320	H_{40}	0.1030	H_{53}	0.1083
		H_{27}	0.12831			H_{54}	0.2468

of CH_3 are expected in the region between 2925 and 3000 cm^{-1} [22] wherein utilising the functional key of B3LYP/6-311++G(d,p), theoretical value are assigned between 3101 and 2993cm^{-1}such that the compounds appear in the region of3101,3094,3082,3055,3027,3014, and 2993 cm^{-1} thereby two peak values are found to be 3027-(99) and 3094 – (97) cm^{-1}for which the PED percentage is listed in the table S2 of the supplementary section [23,24].

4.2.2. Methylene group
Any component of a molecule with the chemical formula CH_2 that is made up of two hydrogen atoms bound to a carbon atom and two single bonds connecting it to the rest of the molecule is commonly known as the methylene group in organic chemistry. The verified record of symmetric and asymmetric range is (3100–2900cm^{-1}) and 3000 cm^{-1} [25].The vibrations of the CH_2 scissoring vibrations and wagging vibrations appears in the regions between 1440 ± 10 and 1340 ± 25 cm^{-1}, respectively [26]. The twisting and rocking modes of the CH_2 group appear in the regions between 1160 ± 20 and 875 ± 25cm^{-1} [27]. With a PED contribution of 57 and 43 percent, respectively, the theoretically calculated values of CH_2 symmetric and asymmetric stretching result in wavenumber at 3055 and 3037 cm^{-1} by the B3LYP/6-311++G(d,p) method, which exactly coincides with experimental observation [28].

4.2.3. Carbon – carbongroup
A covalent bond between two carbon atoms is known as a carbon-carbon bond. The single bond is the most prevalent type. A sigma bond known as a carbon – carbon single bond is created when one hybridised orbital from each carbon atom connects interactions. Usually, the carbon-carbon stretching vibrations take place in the range of 1380–1280 cm^{-1} [29]. The present study has observed the CC bands at 1094 and 1048 cm^{-1}wavelength in the FT-IR region and FT-RAMAN [30]. The bands exhibit

a range of intensities. The theoretical results could be obtained using the B3LYP functional 6-311++G(d,p) level of theory at 1097, 1065, and 1026 cm^{-1} [31]. It illustrates how there is a meaningful compromise between theoretical and experimental data. At its peak, the PED contribution is 71%.

4.2.4. Carbon – oxygengroup
Many inorganic compounds, including oxohalides and carbon oxides, contain carbon – oxygen bonds. A polar covalent bond between carbon and oxygen atoms is known as a carbon – oxygen bond. Significant bands of carbon-oxygen stretching vibrations or linkage can be observed in alcohols and phenols in the 1260–1000 cm^{-1} range [32]. The FT-IR spectrum has a range of around 1091 cm^{-1}. Furthermore, the relevant theoretical values between 1828 and 1095 cm^{-1} are derived using the B3LYP functional 6-311++G(d,p), and they establish a strong correlation with the actual data [33].

4.3. Interaction of energy stability
The Natural Bond Orbital analysis is performed by means of second-order perturbation theory in order to determine the energy and interactions between 'empty' (acceptor) non-Lewis NBOs and 'filled' (donor) Lewis-type NBOs. Making use of the DFT/B3LYP/6-311++G(d,p) level, it is applicable to explain the intramolecular, rehybridization, and delocalisation of electron density in the molecule. An overview of the NBO analysis's findings is provided in Table 1 [34]. The stabilisation energy, E(2), is a key concept in attempts to explain the power of electron donors and acceptors. The stronger the interaction between electron donors and acceptors the greater the degree of conjugation of the entire system which reflects a higher value of stabilisation energy. The hyper conjugative interactions occurring between molecules include $\sigma C_{12}-C_{16} > \sigma^* C_{13}-C_{17}$, $\sigma C_{13}-H_{41} > \pi^* C_{16}-C_{17}, \sigma C_{17}-H_{48} > \sigma^* C_{16}-$
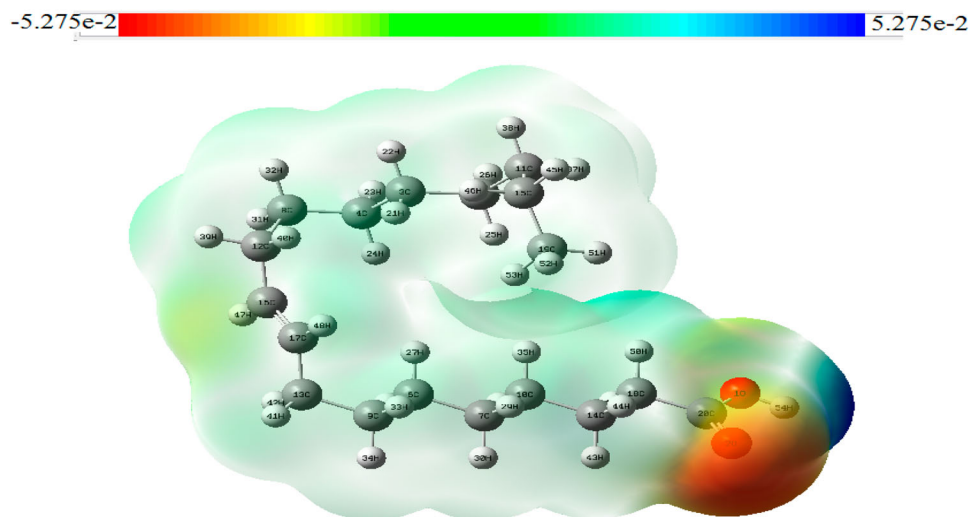
Figure 4. State EvaluationStructure of O9EA.

H_{47}, $\sigma\,C_{18}$–$H_{49} > \pi^*O_2$–C_{20} which are identified to be 4.05,4.16,5.37,5.20 kcal/mol, respectively. The highest bond stability is $LPO_1 > \pi^*O_2$–C_{20} (44.64Kcal / mol) and the lowest bond stability is $\sigma\,C_{13}$–$C_{17} > \sigma^*C_{12}$–C_{16} (4.01Kcal / mol).

4.4. Density of state evaluation

In analyzing the connections between molecular structure and physiochemical properties, the MEP is an extremely useful technique. It represents the net electrostatic effect generated at that location by the molecule's total charge distribution (electron + nuclei) and correlates with dipole moments, electron negativity, partial charges, and chemical reactivity [35]. The total electron density and MEP surfaces of the molecules under study are produced using the B3LYP/6-311++G(d,p) technique. The use of MEP is necessary to comprehend the locations of nucleophilic and electrophilic assault reactions for the study of biological processes and hydrogen bonding interactions [36]. The O9EA's 3D diagram is illustrated in Figure 4. The region displayed on the maps for O9EA has colour codes ranging from 5.275 au (deepest blue) to −5.275 au (deepest red) [37]. MEP can be beneficial in investigating the compound's structural function. It provides important and useful information about charge transfer, the binding process, and reactive regions that are susceptible to attacks by nucleophiles and electrophiles. Differently coloured surfaces have been employed to represent the various reactive areas. Red and blue are the colours that represent electrophilic and nucleophilic reactivity, respectively. The MEP analysis of the molecule reveals promising locations around the NC group, in line with the negative potential areas that have been observed around the nitro group [38].
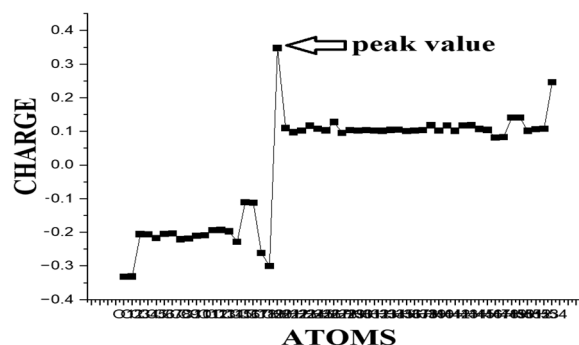

Figure 5. ChargeStructure of O9EA.

4.5. Mulliken population analysis

Determining atomic charges is fundamentally important when implementing quantum mechanical computations for molecular analysis [39].

The charge distribution of the atom indicates that donor and acceptor pairs are created during charge transfer in the molecule [40]. The Mulliken population analysis outcomes for the O9EA molecule using the B3LYP/6-311++G(d,p) basis set are presented in Table 2.

The estimated charges of the O1, O2, and C19 atoms are −0.3314, −0.3312, and −0.2995, respectively. The adjacent C20 atom, which has a strong positive charge of 0.34822, is coupled to these oxygen atoms. This distribution might be the cause of the molecule under discussion's stability. Figure 5 illustrates the charge structure of O9EA.

4.6. UV-Visible spectral analysis

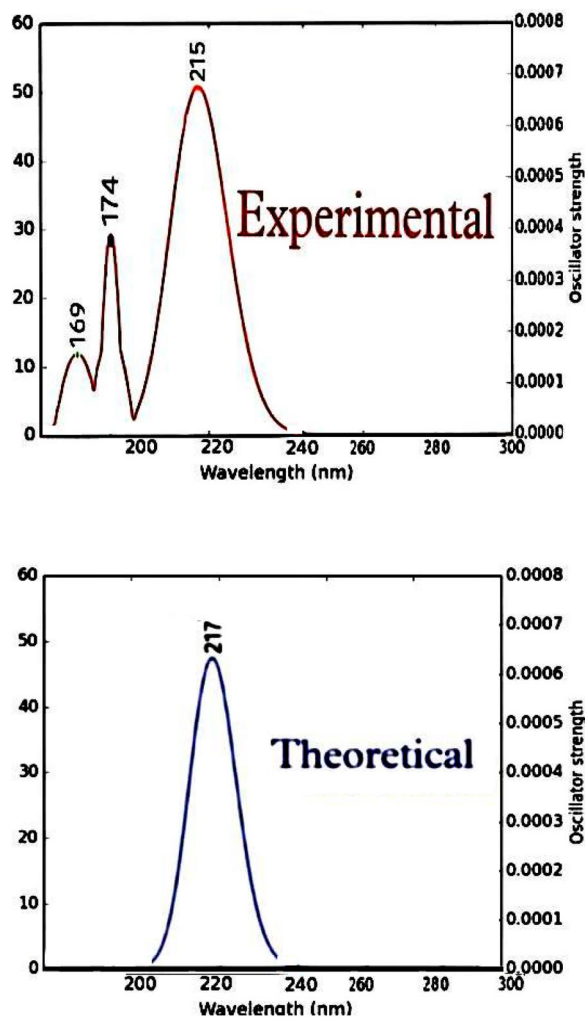The characteristic details of UV-Vis spectral analysis of O9EA is displayed in Table 4 which was computed with

Figure 6. UV-Vis Structure of O9EA.

Table 3. UV-Vis excitation energy of O9EA.

| States | TD B3LYP/6-311++G(d,p) | | | |
| | Gas phase | | | |
	λ_{cal}	E(ev)	Osc. Strength	Expt. obs
S_1	217.89	5.6902	0.0007	215
S_2	176.96	7.0063	0.4563	174
S_3	168.46	7.3597	0.1184	169

reactivity of many organic compounds [43].HOMO-LUMO structure of O9EA is displayed in Figure 7.

The capacity to give an electron is represented by HOMO as it is the highest occupied molecular orbital, while the ability to take an electron is represented by LUMO which is the lowest unoccupied molecular orbital. Table 4 lists the electrical properties of O9EA.

The Eigen values of the HOMOs (p donor) and LUMOs (p acceptor), as well as their energy gap, also shows the chemical activity. Utilising the energy difference between HOMO and LUMO, the bioactivity resulting from intramolecular charge transfer has recently been demonstrated [44]. It is possible to use the HOMO-LUMO energy esteems to make them closely associated with the molecules' electron affinity (j) and ionisation potential (i). Furthermore, for the Octadec-9-Enoic Acid molecules, other parameters have been predicted, including Chemical Potential (µ), Chemical Hardness (η), Chemical Softness (δ), Electronegativity (χ), Electrophilicity (ω), Electron acceptor power (ω^+), and Electron donor power (ω^-). The proposed HOMO energy can be directly influenced by a compound's ionisation potential. However, LUMO energy can also be thought of as an outcome made up of the electrons, in which case it is considered a direct contribution that results from the electron affinity [45]. Additionally, two notable molecular orbitals that make up HOMO-LUMO can be studied in order to better comprehend the molecular characteristics that HOMO and LUMO represent. Energy value of Homo-Lumo of O9EA is represented in Figure 8.

6. Molecular docking

A popular computational technique for figuring out the covalent and non-covalent interactions between small molecules and macromolecules, such as proteins, enzymes, and DNA, is molecular docking. It is the most dependable and appropriate approach for ligand – and structure-based drug design. Molecular docking studies have been performed utilising the Maestro-10.2 docking programme inbuilt in Schrödinger suite. Before conducting an experimental synthesis, computational screening of biological and biochemical molecules can be a simple and economical method [46,47]. On these counts,

the B3LYP/6-311++G(d,p) approach in furtherance to the observed UV-Vis data. The UV radiation obtained reveals the wavelength at which molecules absorb electrons to make a transition from an excited to the ground state [41].

Measurements performed of the O9EA molecule, which was initially identified in a methanol solvent, between 200 and 260 nm are illustrated in Figure 6 to shed light on the nature of its electronic transitions. Table 3 for UV-Vis absorption indicates three probable projected transitions, with gas phase absorption maxima at 217.89, 176.96, and 168.46 nm, respectively [42]. It is quite evident from the analyses of experimental and theoretical that they corroborate with each other.

5. Electronic properties (*HOMO – LUMO*)

The concepts of aromaticity, HOMO, and LUMO are essential for comprehending the chemical stability and

Figure 7. HOMO-LUMOStructure of O9EA.

Table 4. Electrical properties of O9EA.

Variable	Set Expression	Evaluation
HOMO energy (i)	I	6.32
LUMO energy (j)	J	1.03
Energy gap (eV)	Eg = HOMO – LUMO	5.29
Ionisation potential (I)	– (HOMO)	−6.32
Electron affinity (A)	– (LUMO)	−1.03
Chemical Hardness (η)	1/2(LUMO-HOMO) = 1/2 (i-j)	2.64
Chemical Softness (δ)	$1/\eta$	0.37
Chemical potential (μ)	1/2(LUMO + HOMO) = 1/2 (i + j)	−7.35
Electrophilicity (ω)	$\mu^2 / 2\eta$	10.23
Electronegativity (χ)	(LUMO + HOMO)−μ	7.35
Electron acceptor power(ω+)	$(i + 3j)^2$ / 16 (i–j)	1.04
Electron donor power (ω-)	$(3i + j)^2$ / 16 (i–j)	4.72

molecular docking methodology is employed to probe the interaction between acetylcholinesterase and butyrylcholinesterase using the $C_{18}H_{34}O_2$ molecule. The docked pose of the $C_{18}H_{34}O_2$ molecule is at its lowest energy. Investigating the ligplot interaction reveals a hydrogen bond between the O-atom of acetylcholinesterase's Leusine Leu and the H-atom of the aromatic ring of the $C_{18}H_{34}O_2$ molecule. It can be inferred that the $C_{18}H_{34}O_2$ molecule make chains with rings of Leu, Ala, and Phe such that hydrophobic interactions are formed. However, as seen in the ligplot of butyrylcholinesterase, only Vander Waal's interactions with the $C_{18}H_{34}O_2$ molecule
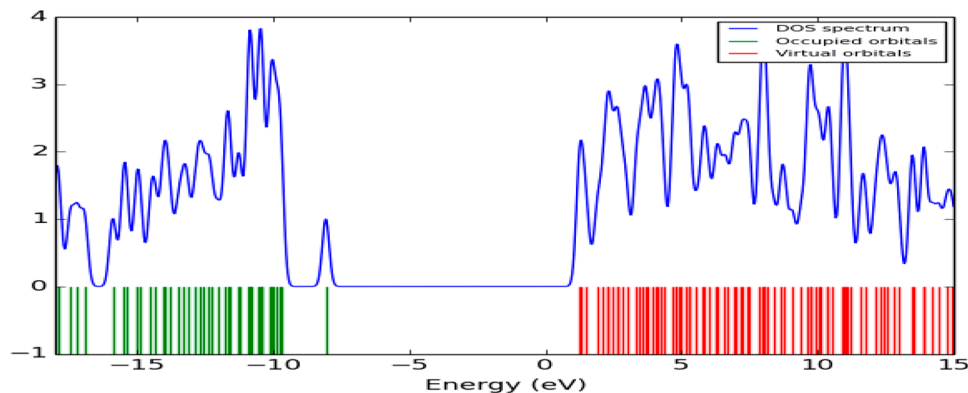
Figure 8. Energy Value of Homo- Lumoof O9EA.

were provided by butyrylcholinesterase. Moreover, the binding results suggest that the various mode of interaction occurring via H-bond, π-π stacking, Van der Waals, and electrostatic interaction are significantly prominent. Acetylcholinesterase exhibited a higher binding constant and greater spontaneity of reaction as a result of more significant interactions. Based on molecular docking data, several electronic and steric descriptors have been computed for a comprehensive understanding of macroscopic interaction. The electron-donating and electron-accepting characteristics of a compound are measured by the energies of its frontier molecular orbitals, or EHOMO and ELUMO [48]. The observed binding energy is 3.54 and the protein is indentified by (PBD) a bond distance of 2 Å while the bonded residue of THR 153 is witnessed. Since the compounds offer electrons to those with higher EHOMO values, they are regarded as strong electron donors, and compounds with lower ELUMO values have a greater propensity to accept electrons. Because of its larger EHOMO in this study compared to its smaller EHOMO in its interaction with Acetylcholinesterase, the $C_{18}H_{34}O_2$ molecule donates electrons during its association with Butylcholinesterase. The $C_{18}H_{34}O_2$ molecule withdraws electrons from the acetylcholinesterase residues when it forms a network with the enzyme, resulting in strong interactions and high binding strength, which raises the binding constant value. The steric descriptors that were computed based on the simulation outcomes consisted of hydrophobic surface volume, heat of formation, and molar refractivity. The measurement of molecular polarizability, or MR, was found to be higher for acetylcholinesterase, indicating a greater binding strength between the enzyme and the $C_{18}H_{34}O_2$ molecule. Stable and strong complexes also had smaller positive values for heat of formation. Comparing acetylcholinesterase to butyrylcholinesterase in this work, the former has a higher binding constant, stronger complex formation, and a smaller positive heat of formation value. Additionally, it was found

that because compound PB has a higher hydrophobic surface contact with acetylcholinesterase than butyrylcholinesterase, acetylcholinesterase has a relatively larger hydrophobic surface volume than butyrylcholinesterase. A larger amount of enzyme residues are overlapping the $C_{18}H_{34}O_2$ molecule, which is responsible for the higher hydrophobic surface area. The compound exhibits a single hydrogen bond (distance of 1.99 Å) and an active mode of interaction with the HSA receptor. Moreover, hydrophobic interactions with acetic, decanoic, and formic acids are involved. A higher activity against the receptor human serum albumin is demonstrated by the docking results. Figure 9 illustrates the molecular Docking of O9EA.

7. NLO properties

The results of potentially measured values of the average dipole moment (μ), polarizability (α), and first-order hyperpolarizability (β) of O9EA organic molecules are analyzed. For O9EA, the mean polarizability and dipole moments are calculated to be 4×10^{-23} e.s.u. and 1.82 Debye, respectively. The title compound chemical's and urea's reference substance's first-order hyperpolarizability (β) is compared such that the computed values are 0.93×10^{-30} e.s.u and 0.3728×10^{-30} esu, respectively [49]. The title chemical's calculated β values are higher than that of urea, suggesting that the molecules have favourable NLO characteristics.

8. RDG analysis

According to PASS Online's prediction and previous investigation on comparable compounds that are related to NAEF, the intended objective of this reduced density gradient (RDG) study is to learn more about the intermolecular interactions from the crystal packing concerning the molecular docking investigations against alcoholic cirrhosis illness [50]. Alcoholic cirrhosis is a severe
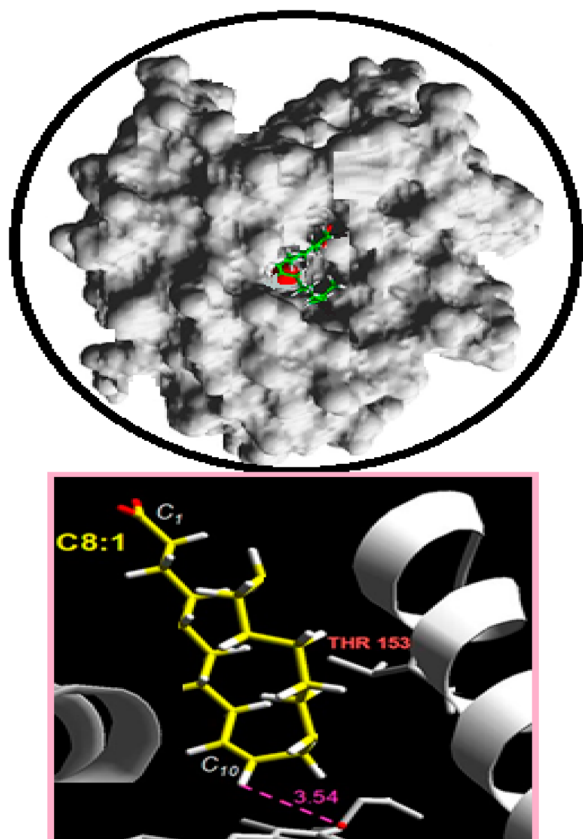
range of 0.4065–0.2419 a.u. (O1–C7 to C3–C5). The electrons densities of N2–C4 and C3–C5 are 0.2538 and 0.2419 a.u., respectively, while O1–C7 and C6 = C8 have high densities of 0.4065 and 0.3431 a.u., respectively. The stronger bond ellipticity (ϵ = 0.3426 a.u.) at C6 = C8 is a result of the effect of double bond attachments between the carbon atoms, and it has been used to identify the increased unequal distribution of electrons in the prevailing molecule NAEF. This characteristic quantifies the π-bond and symbolises the anisotropy of the electron density's curvature. The electron density distribution's asymmetry and strongest π-delocalisation are revealed by the highest value. RDG analysis is a visual method that improves the detail of NCI and covalent interactions [52]. Figure 10 displays the scatter plot and image of the gradient isosurfaces for the NAEF. The RDG scatter spectra's three colours – red, green, and blue – indicate that the function of (λ_2) ρ lies between 0.05 and 0.05 a.u., where the green peak (between 0.008 and 0.0185 a.u.) and the red peak (between 0.009 and 0.0195 a.u.) represent the van der Waals force and the steric forces between the compound's atoms, respectively. This graph illustrates the van der Waals forces between the molecule's C6 = C8 & C4–H12 and C5–H13 & C3–10 groups, as well as the steric effects between the C7–O1 & C4–N2 and C3–H9 & C7–N2 groups. Owing to the lack of blue spikes, all interactions in NAEF are made solely through covalent bonds, and this is consistent with the results of bond categorisation studies conducted by AIM and the findings of gas phase electron density. No non-covalent areas have been observed in NAEF.

9. ^{1}H and ^{13}C NMR spectra

One of the key instruments for characterising molecules is the application of ^{1}H and ^{13}C NMR spectroscopy. The Bruker Ac DPX-200 (300 MHz) spectrometer was employed to obtain the ^{1}H and ^{13}C NMR spectra of the $C_{18}H_{34}O_2$ molecules using CDCl3 as the solvent. The ^{1}H and ^{13}C chemical shift values from GIAO (gauge-independent atomic orbitals) are compared to the experimental results. The latter was calculated using the 6-311++G(d,p) basis set and the B3LYP functional.^{1}H and ^{13}C NMR ofO9EA are displayed in Figure 11.

Tetramethylsilane (TMS) and $C_{18}H_{34}O_2$'s geometry were fully optimised in tandem. The ^{1}H and ^{13}C NMR chemical shifts of the compound were converted to the TMS scale by subtracting the calculated absolute chemical shielding of TMS, with values of 31.8821 ppm (^{1}H) and 182.466 ppm (^{13}C) for B3LYP/6-311++G (d,p). The obtained results enabled us to compare the theoretical ^{1}H NMR chemical shifts with the experimental data. Results from experiments and theoretical analysis are combined.

Figure 9. Molecular Dockingof O9EA.

type of liver disease brought on by heavy, prolonged alcohol consumption. If someone gets cirrhosis from alcohol, their liver has most likely not been functioning normally for a very long time; as a result, it becomes swollen, rigid, and barely functional. As shown in Figure 10, the molecular graphs of the NAEF molecule were analyzed using the AIM method and the AIMALL tool. The nature and strength of interactions between natural bonds as well as intramolecular interactions between molecules can be better understood by looking into the aforementioned subjects. The electron densities (ρ(r)) and their Laplacian $\nabla 2\rho$(r), the local potential electron energy density (V(r)), the kinetic electron density (G(r)), and the total electron energy densities (H(r)) at the bond critical points (BCP) are some of the topological details that are highlighted. These are the points through which the electrons are transferred or shared to create electrostatic or covalent bonds, which can be used in this analysis to characterise the nature of the interactions [51] such as covalent, weak electrostatic, and non-covalent bond integrations. In the case of NAEF, all of the negative symbols of $\nabla 2\rho$(r) show that there are neither closed-shell interactions nor non-covalent bonds exist. The electron density ρ(r) indicates shared-shell contact (strong covalent bonds) between the bonds in the current molecule and is reported in the
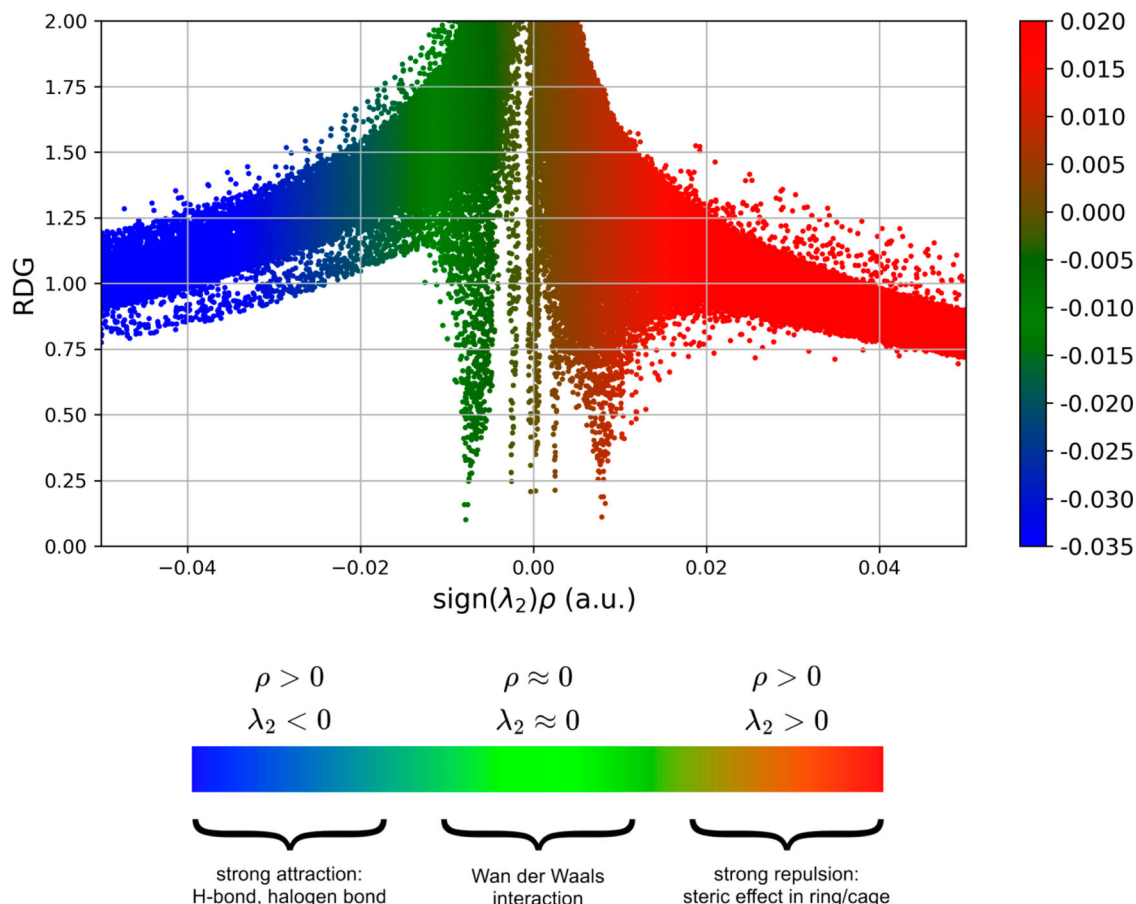
Figure 10. RDG of O9EA.

The appearance of singlet two peaks of OCH3 at 3.79 and 3.89 ppm amply demonstrated the formation of the $C_{18}H_{34}O_2$.

Observe that, subsequent to the delocalisation of the free doublet of oxygen produced by the group imino (C1/4N), the chemical shift of the protons of the methoxy group (O–CH3) is de-blinded. The observed values of the peaks mentioned are 3.49–3.96 ppm and 3.61–3.98 ppm, respectively, which correspond to their theoretical values. The calculated values are observed at 6.61–8.24 ppm in the ^{1}H NMR spectrum, while the aromatic proton signals appear as a mutiplet at 6.75–8.13 ppm regions. The experimentally observed peak of the methane proton exo-cyclic is 7.70 ppm, while the computed peak is located at 7.62 ppm. Protons from H6 and H2 may be responsible for the signals seen at 8.41 and 8.43 ppm, respectively, in proximity to the nitro group. In contrast, carbonyl carbon atoms are detected in the title compound's ^{13}C NMR spectra at 169.69 ppm. Theoretically, this value is observed at 160.53 ppm [53].

Methoxy group carbons (C23 and C24) are calculated to be 53.88 and 53.55 ppm, respectively; experimental observations show that these values are to be at 55.98 and 55.90 ppm as indicated by the observed results of the experiment. Moreover, the molecular environmental shift may be because of the slight changes.

10. Conclusion

Using the 6-311++G(d,p) basis set, the DFT-B3LYP method was used in the current work to optimise the geometry of the compound named O9EA. Bond length, bond angle, and other molecular structural parameters, Mulliken DFT calculations have yielded the vibrational frequencies and atomic charges of the optimised geometry's fundamental modes. The potential energy distribution is the basis for assigning wave numbers in the complete form based on vibration (PED). It was possible to get a good correlation between the
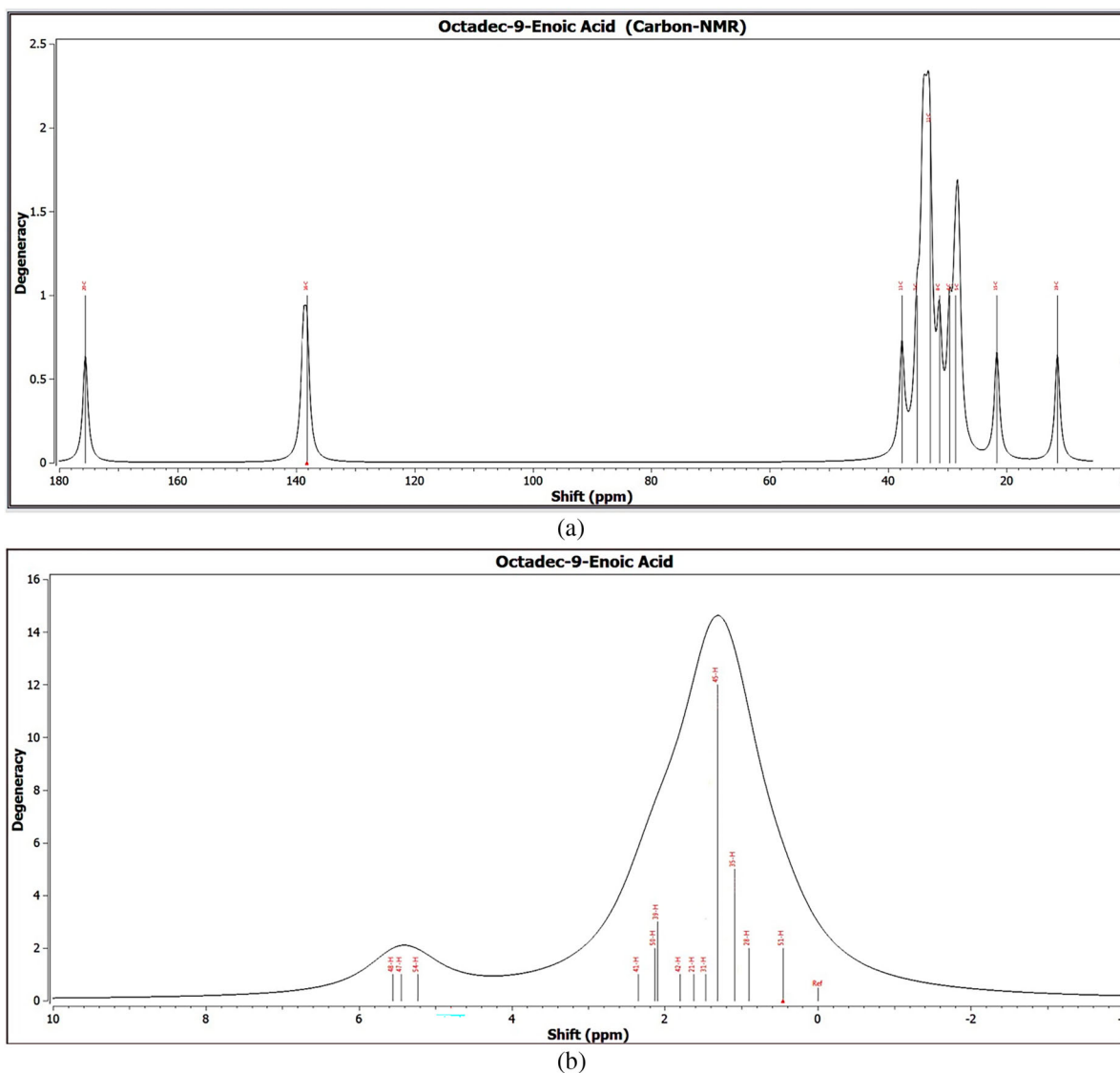
Figure 11. a. ^{13}CNMR of O9EA. b. ^{1}HNMR of O9EA.

theoretical and experimental frequencies. The energy gap HOMO–LUMO has been computed. The locations of nucleophilic reactions and electrophilic attacks are shown by the MEP analysis. By making use of NBO calculations, the formation of hydrogen bonds was examined with respect to charge density. The DFT calculations and UV spectra were employed to determine the electronic structure and the absorption band assignments, respectively. The Fukui function demonstrates the identification of the electrophilic and nucleophilic attack sites. We anticipate that all those who are interested in the experimental and theoretical details of the title molecule will find the study's findings beneficial. The targeted active site of the ulcer protein has been identified based on molecular docking studies.

Credit authorship contribution statement

C. Prabhu: Conceptualization, Methodology, Validation, Formal analysis, Writing – original draft, editing, Visualization. **P. Rajesh:** Investigation, Supervision, Project administration, review, editing. **M. Lawrence:** Conceptualization, Software, Resources, Project administration, Writing, review; editing. **S. Sahaya Jude Dhas:** Conceptualization, Software, Investigation, Project administration, Formal analysis, Methodology, Validation. **Abdulrahman I. Almansour:** Conceptualization, Methodology, Validation, Formal analysis.

Disclosure statement

No potential conflict of interest was reported by the author(s).

Funding

Data availability statement

Data will be made available on request.

References

[1] P.B. Rajsekhar, R.S. Arvind Bharani, K. Jini Angel, Maya Ramachandran, and Sharadha Priya Vardhini Rajasekhar, J. Chem. Pharm. Res. **8** (1), 351–355 (2016).

[2] K. RaveendraRetnam and A. John De Britto, Nat. Prod. Rad. **6** (5), 386–390 (2007).

[3] A.O. Afolabi, E.T. Oluwakanmi, H.M. Salahdeen, A.O. Oyekunle and I.A. Alagbonsi, J. Med. Med. Res. **4** (1), 322–330 (2014). doi:10.9734/BJMMR/2014/4217

[4] K. Jaikumar, M. Sheik Noor Mohamed, S. Marimuthu, S. Anantha Padmanabhan, D. Anand and P. Saravanan, Indo Am J. Pharm. Res., **6** (12) 2231–6876 (2016).

[5] V. Vorobyova1 and M. Skiba, J. Chem. Technol. Metall. **55** (1), 210–222 (2020).

[6] D.O. Onukwuli and O. Monday, J. Chem. Technol. Metall. **51** (3), 302–314 (2016).

[7] D.J. Newman and G.M. Cragg, J. Nat. Prod. **70**, 461–477 (2007). doi:10.1021/np068054v

[8] S. Sahoo, D.M. Kar1 and S. Mohapatra, Indian J. Pharm. Sci. **68** (5), 653–655 (2006). doi:10.4103/0250-474X.29640

[9] A.D. Becke, J. Chem. Phys. **98**, 5648–5652 (1993). doi:10.1063/1.464913

[10] M.A. Hashmi, A. Khan, K. Ayub and U. Farooq, Spectrochim. Acta, Part A. **128**, 225–230 (2014). doi:10.1016/j.saa.2014.02.163

[11] M. Lawrence, P. Rajesh, M. Thirunavukkarasu and S. Muthu, J. Mol. Liq. **382**, 121940 (2023). doi:10.1016/j.molliq.2023.121940

[12] M.H. Jamróz, Spectrochim. Acta. A. **114**, 220 (2013). doi:10.1016/j.saa.2013.05.096

[13] M. Lawrence, P. Rajesh, M. Vimala, R. Girija and S. Sahaya Jude Dhas, Mol. Phys. (2023). doi:10.1080/00268976.2023.2264399.

[14] A. Djafri, A. Chouaih, J.C. Daran, A. Djafri and F. Hamzaoui, ActaCryst E. **73**, 511–514 (2017).

[15] K. Shobana, E. Sailatha, S. Gunasekaran, P. Rajesh, S. Srinivasan, M. Raja and P.P. Moorthi, Int. J. Sci. Technol. Res. **8** (09), 266–275, (September 2019). ISSN 2277-8616.

[16] Y. Takano and K.N. Houk, J. Chem. Theory. Comput. **1** (1), 70–77 (2005).

[17] M.H. Jamroz, *Vibrational Energy Distribution Analysis* (VEDA 4 Computer Program, Poland, 2004).

[18] G. Socrates, *Infrared Characteristic Group Frequencies* (Wiley-Interscience Chichester, New York, U.K., 1980).

[19] N. Roeges, *A Guide to the Complete Interpretation of Infrared Spectra of OrganicStructures* (Wiley, New York, 1994).

[20] A.F. Shestakov, D.V. Konarev, S.V. Simonov, S.S. Khasanov, A.N. Lapshin and N.F. Goldshleger, RSC Adv. **3** (22), 8341–8350 (2013). doi:10.1039/c3ra22787a

[21] S. Celik, A.T. Albayrak, S. Akyuz and A. E. Ozel, J. Biomol. Struct. Dyn. **37** (10), 2515–2526 (2019). doi:10.1080/07391102.2018.1495578

[22] M. Govindarajan, K. Ganasan, S. Periandy and M. Karabacak, Spectrochim. Acta A. **79**, 646–653 (2011). doi:10.1016/j.saa.2011.03.051

[23] N. Sundaraganesan, G. Elanga, S. Sebastian and P. Subramani, Indian J. Pure Appl. Phys. **47**, 481–490 (2009).

[24] M. Lawrence, P. Rajesh and S. Sahaya Jude Dhas, J Pharm. Negat. Results. **13** (10), 1495–1513, (2022).

[25] Velraj, S.Soundharam and C.Sridevi, J. Mol. Struct. **1060**, 156–165 (2014). doi:10.1016/j.molstruc.2013.12.040

[26] N.B. Colthup, L.H. Daly and S.E. Wiberly, *Introduction to Infrared and Raman Spectroscopy* (Academic Press, New York, 1990).

[27] N.P.G. Roeges, *A Guide to the Complete Interpretation of Infrared Spectra of Organic Compounds* (Wiley, New York, 1994).

[28] P.B. Nagabalasubramanian, M. Karabacak and S. Periandy, Spectrochimic. Acta. **85**, 43–52 (2012). doi:10.1016/j.saa.2011.09.001

[29] R.M. Silverstein and G.C. Bassler. Spectrometric Identification of Organic Compounds, J. Chem. Educ. **39** (11), 546 (1962). doi:10.1021/ed039p546

[30] N.P.G. Roeges, *A Guide to the Complete Interpretation of Infrared Spectra of Organic Structures* (John Wiley and Sons Inc, New York, 1994).

[31] G. Varsanyi, *Assignments of Vibrational Spectra of Seven Hundred Benzene Derivatives* (Wiley, New York, 1974).

[32] D.N. Sathyanarayana, *Vibrational Spectroscopy Theory and Applicaions* (Age International Ltd, New Delhi, India, 2011), 422.

[33] R.M. Silverstein and F.X. Webster, *Spectroscopic Identification of Organic Compounds* 6th ed. (John Wiley & Sons, Canada, 1998), 90.

[34] J. Liu, Z. Chen and S. Yuan, J. Zhejiang Univ. Sci. B. **6**, 584–589 (2005). doi:10.1631/jzus.2005.B0584

[35] E.J. Luque, J.M. Lopez and M. Orozco, Theor. Chem. Acc. **103**, 343–351 (2000). doi:10.1007/s002149900013

[36] P. Politzer, J.S. Murray, D.L. Beveridge and R. Lavery, editors, *Theoretical Biochemistry, and Molecular Biophysics: A Comprehensive Survey, Protein, vol. 2* (Adenine Press, Schenectady, New York, 1991).

[37] R.M. Silverstein, G.C. Bassler and T.C. Morill, *Spectrometric Identification of Organic Compounds*, 4th ed. (Wiley, New York, 1981).

[38] M. Lawrence, P. Rajesh, A. Irfan and S. Muthu, J. Mol. Liq. **388**, 122744 (2023). doi:10.1016/j.molliq.2023.122744

[39] B. Lambert, *Introduction to Organic Spectroscopy* (Mac millan Publjcation, New York, 1987).

[40] R.S. Mulliken, J. Chem. Phys. **23**, 1833–1840 (1995). doi:10.1063/1.1740588

[41] A. Manikandan, et al., Int. J Chem Tech Res. **11** (09), 308–321 (2018). doi:10.20902/IJCTR.2018.110937.

[42] P. Rajesh, S. Gunasekaran, S. Seshadri and T. Gnanasambandan, Spectrochim. Acta, Part A. **132**, 249–255 (2014). doi:10.1016/j.saa.2014.04.106

[43] I. Fleming, *Frontier Orbitals and Organic Chemical Reactions* (John Wiley &Sons, New York, 1976).

[44] N.C. Handy, P.E. Maslen, R.D. Amos, J.S. Andrews, C.W. Murry and G. Laming, J. Chem. Phys. Lett. **197**, 506–515 (1992). doi:10.1016/0009-2614(92)85808-N

[45] C.C. Ersanli, G.K. Kantar and S.S. Maz, J. Mol. Struct. **1143**, 318–327 (2017). doi:10.1016/j.molstruc.2017.04.032

[46] R. Rahmani, N. Boukabcha, A. Chouaih, F. Hamzaoui and S. Goumri-Said, J. Mol. Struct. **1155**, 484–495 (2018). doi:10.1016/j.molstruc.2017.11.033

[47] P. Fouzia, et al., PLoS One. **13** (10), e0205764 (2018).

[48] T. Akram, M.A. Abbasi, A. Mahmood, E. Barboza de Lima, F. Perveen, M. Ashraf, I. Ahmad and S. Goumri-Said, J. Mol. Struct. **1195**, 119–130 (2019). doi:10.1016/j.molstruc.2019.05.065

[49] P.V. Ramana, T. Sundius, S. Muthu, K.C. Mouli, Y.R. Krishna, K.V. Prasad, R.N. Devi, A. Irfan and C. Santhamma, J. Mol. Struct. **1253**, 132211 (2022). doi:10.1016/j.molstruc.2021.132211

[50] H. Jiang, X. Zhang, J. Shen, Y. Zhang, Y. Gu, T. Tian, M. Chu, X. Zhuang and Y. Lian, Int. Arch. Occup. Environ. Health. **92**, 967–975 (2019). doi:10.1007/s00420-019-01436-1

[51] M. Thirunavukkarasu, P. Prabakaran and A. Saral, J. Mol. Liq. **380**, 121714 (2023). doi:10.1016/j.molliq.2023.121714

[52] J.R. Cheeseman, G.W. Trucks, T.A. Keith and M.J. Frisch, J. Chem. Phys. **104**, 5497–5509 (1996). doi:10.1063/1.471789

[53] A. Djafri, F. Perveen, N. Benhalima, N. Khelloul, R. Rahmani, A. Djafri, A. Chouaih, M.B. Kanoun and S. Goumri-Said, doi:10.1016/j.heliyon(6)2020.e05754.